

Symmetry of $k \cdot p$ Hamiltonian in pyramidal InAs/GaAs quantum dots: Application to the calculation of electronic structure

Nenad Vukmirović,* Dragan Indjin, Vladimir D. Jovanović, Zoran Ikonić, and Paul Harrison

*School of Electronic and Electrical Engineering,
University of Leeds, Leeds LS2 9JT, United Kingdom*

(Dated: November 20, 2018)

A method for the calculation of the electronic structure of pyramidal self-assembled InAs/GaAs quantum dots is presented. The method is based on exploiting the \overline{C}_4 symmetry of the 8-band $k \cdot p$ Hamiltonian with the strain taken into account via the continuum mechanical model. The operators representing symmetry group elements were represented in the plane wave basis and the group projectors were used to find the symmetry adapted basis in which the corresponding Hamiltonian matrix is block diagonal with four blocks of approximately equal size. The quantum number of total quasi-angular momentum is introduced and the states are classified according to its value. Selection rules for interaction with electromagnetic field in the dipole approximation are derived. The method was applied to calculate electron and hole quasibound states in a periodic array of vertically stacked pyramidal self-assembled InAs/GaAs quantum dots for different values of the distance between the dots and external axial magnetic field. As the distance between the dots in an array is varied, an interesting effect of simultaneous change of ground hole state symmetry, type and the sign of miniband effective mass is predicted. This effect is explained in terms of the change of biaxial strain. It is also found that the magnetic field splitting of Kramer's double degenerate states is most prominent for the first and second excited state in the conduction band and that the magnetic field can both separate otherwise overlapping minibands and concatenate otherwise nonoverlapping minibands.

Introduction

Semiconductor quantum dots made by Stranski-Krastanow growth have attracted great interest over the past few years from the view of fundamental physics, as well as due to their application in optoelectronic and microelectronic devices. In order to understand the physics of quantum dots and model and design such devices the electronic structure needs to be accurately known. The large lattice mismatch between InAs and GaAs has enabled the fabrication of quantum dots putting it at the forefront of both theoretical and experimental research. Different quantum dot shapes (such as pyramid¹, lens² and disk³) of InAs/GaAs self-assembled quantum dots are often reported.

A range of theoretical approaches has been used so far to calculate the energy levels in self-assembled quantum dots - effective mass^{4,5,6,7}, $k \cdot p$ ^{8,9,10,11} and the pseudopotential method^{12,13}. In quantum dots with cylindrical symmetry, symmetry considerations have been applied to effectively reduce the geometry of the problem from three-dimensional to two-dimensional, both in the effective mass and the $k \cdot p$ method (within the axial approximation)¹⁴. The possible symmetries of the states in hexagonal III-nitride quantum dots have recently been determined¹⁵. The symmetry of the pyramid has been used in the effective mass calculation¹⁶ to reduce the size of the corresponding Hamiltonian matrix,

however in none of the $k \cdot p$ calculations of pyramidal quantum dots has the explicit use of the symmetry of the Hamiltonian been reported. The aim of this paper is to exploit the symmetry in $k \cdot p$ calculation of the electronic structure of pyramidal InAs/GaAs quantum dots.

The symmetry of a pyramidal InAs/GaAs quantum dot when a full atomistic structure is considered is \overline{C}_{2v} and is lower than the symmetry of the dot's geometrical shape¹³. Due to the computational complexity of the pseudopotential methods that take into account the atomistic nature of the structure, one often employs the $k \cdot p$ method which is considered to be a reliable tool for modeling the electronic structure of quantum dots despite its known limitations⁸. The symmetry of the $k \cdot p$ model itself is the symmetry group of the zincblende crystal lattice. When the model is applied to pyramidal quantum dots the symmetry group is the intersection of the geometrical symmetry of the pyramid shape and the zincblende bulk symmetry. Since the pyramid shape symmetry group is a subgroup of the symmetry of the zincblende crystal lattice, it follows that the symmetry group of the model is the double \overline{C}_4 group¹⁷. Two different approaches are used to calculate the strain distribution in quantum dots - the continuum mechanical^{8,11} and the valence force field model^{8,10}. When the strain distribution is incorporated in the $k \cdot p$ method, the continuum mechanical model preserves the \overline{C}_4 symmetry, while the valence force field model, due to its atomistic nature, breaks it^{8,10}. Nevertheless, the comparisons of the two models have shown that they give similar results^{8,18}. In this paper, we apply the 8-band $k \cdot p$ method with the strain taken into account via the continuum mechanical model. We shall refer to this in the rest of the text for brevity as the model. Therefore, the symmetry group of this model is \overline{C}_4 . All the results presented in Sec. III are strictly valid in the framework of such an idealized model.

In previous years, arrays of vertically stacked quantum dots with 10 or more layers have been reported^{19,20}. The quantum wire behavior of such structures was theoretically investigated in Ref. 9. Most of the theoretical investigations of the InAs quantum dots in a magnetic field have focused on the dots with a parabolic confinement potential^{21,22,23,24,25,26,27} or just on the conduction band states^{16,28}. More recently, the influence of a magnetic field on pyramidal single quantum dots has been investigated in the framework of the $k \cdot p$ method²⁹.

This paper is organized as follows. In Sec. I the relations necessary to apply the plane wave expansion method³⁰ to 8-band $k \cdot p$ calculation of quantum dots based on materials with zincblende crystal symmetry in the presence of strain and external axial magnetic field are given. In Sec. II the representations of the symmetry group elements, the reduction of the representation to its irreducible constituents and finally the symmetry adapted basis are found. The states are classified according to their symmetry and selection rules for absorption of electromagnetic radiation in the dipole approximation are found. It is also shown how symmetry considerations can be incorporated into the plane wave method. Finally, in Sec. III the method presented is applied to calculate the electron and hole quasibound states in a periodic array of vertically stacked pyramidal self-assembled InAs/GaAs quantum dots for different values of the period of the structure and in the presence of an external axial magnetic field.

I. THE PLANE WAVE METHOD

In the presence of an axial magnetic field the total 8-band $k \cdot p$ Hamiltonian is a sum of the kinetic part of the Hamiltonian \hat{H}_k , the strain part \hat{H}_s , the modification of the kinetic

part due to magnetic field \hat{H}_B and the Zeeman part \hat{H}_Z

$$\hat{H} = \hat{H}_k + \hat{H}_s + \hat{H}_B + \hat{H}_Z. \quad (1)$$

The state of the system within the framework of the 8-band $k \cdot p$ method is given as a sum of slowly varying envelope functions $\psi_i(\mathbf{r})$ multiplied by the bulk Bloch functions $|i\rangle$ (Eq. 4), i.e.

$$|\Psi\rangle = \sum_{i=1}^8 \psi_i(\mathbf{r})|i\rangle. \quad (2)$$

The eigenvalue problem of the 8-band $k \cdot p$ Hamiltonian \hat{H} can therefore be written as

$$\sum_{j=1}^8 H_{ij} \psi_j(\mathbf{r}) = E \psi_i(\mathbf{r}). \quad (3)$$

The basis of Bloch functions $|J, J_z\rangle$ (where $\hat{\mathbf{J}}$ is the total angular momentum of the Bloch function) used to represent the Hamiltonian is given by³¹

$$\begin{aligned} |1\rangle &= \left| \frac{1}{2}, -\frac{1}{2} \right\rangle = |S \downarrow\rangle, \\ |2\rangle &= \left| \frac{1}{2}, \frac{1}{2} \right\rangle = |S \uparrow\rangle, \\ |3\rangle &= \left| \frac{3}{2}, -\frac{3}{2} \right\rangle = -\frac{i}{\sqrt{2}} |(X - iY) \downarrow\rangle, \\ |4\rangle &= \left| \frac{3}{2}, -\frac{1}{2} \right\rangle = \frac{i}{\sqrt{6}} |(X - iY) \uparrow\rangle + i\sqrt{\frac{2}{3}} |Z \downarrow\rangle, \\ |5\rangle &= \left| \frac{3}{2}, \frac{1}{2} \right\rangle = -\frac{i}{\sqrt{6}} |(X + iY) \downarrow\rangle + i\sqrt{\frac{2}{3}} |Z \uparrow\rangle, \\ |6\rangle &= \left| \frac{3}{2}, \frac{3}{2} \right\rangle = \frac{i}{\sqrt{2}} |(X + iY) \uparrow\rangle, \\ |7\rangle &= \left| \frac{1}{2}, -\frac{1}{2} \right\rangle = -\frac{i}{\sqrt{3}} |(X - iY) \uparrow\rangle + \frac{i}{\sqrt{3}} |Z \downarrow\rangle, \\ |8\rangle &= \left| \frac{1}{2}, \frac{1}{2} \right\rangle = -\frac{i}{\sqrt{3}} |(X + iY) \downarrow\rangle - \frac{i}{\sqrt{3}} |Z \uparrow\rangle. \end{aligned} \quad (4)$$

The kinetic and the strain part of the Hamiltonian in the basis (4) are given in Ref. 31 and the matrix elements of the 8-band $k \cdot p$ Hamiltonian in the case of a magnetic field of arbitrary direction are given in Ref. 32. In the case of the axial magnetic field that we are interested in, the influence of the magnetic field B can be taken into account by replacing k_i with $k_i + \frac{e}{\hbar} A_i$ in the kinetic part of the Hamiltonian, where A_i is the i -th component of the magnetic vector potential, and by adding the Zeeman term \hat{H}_Z (Ref. 32). We take the symmetric gauge for the vector potential $\mathbf{A} = \frac{1}{2}B(-y, x, 0)$.

The plane wave method is based on embedding the quantum dot in a box of sides L_x , L_y and L_z (Fig. 1) and assuming the envelope functions are a linear combination of plane

waves

$$\psi_i(\mathbf{r}) = \sum_{\mathbf{k}} A_{i,\mathbf{k}} \exp(i\mathbf{k} \cdot \mathbf{r}), \quad (5)$$

with the coefficients $A_{i,\mathbf{k}}$ to be determined. The wave vectors taken in a summation are given by $\mathbf{k} = 2\pi \left(\frac{m_x}{L_x}, \frac{m_y}{L_y}, \frac{m_z}{L_z} \right)$ ($m_x \in \{-n_x, \dots, n_x\}$, $m_y \in \{-n_y, \dots, n_y\}$, $m_z \in \{-n_z, \dots, n_z\}$). The number of plane waves taken is thus $N = 8(2n_x + 1)(2n_y + 1)(2n_z + 1)$, where $2n_t + 1$ is the number of plane waves per dimension t ($t \in \{x, y, z\}$). Due to the symmetry of the pyramid, the embedding box sides L_x and L_y are taken to be equal ($L_x = L_y$), as well as the number of plane waves per dimensions x and y ($n_x = n_y$).

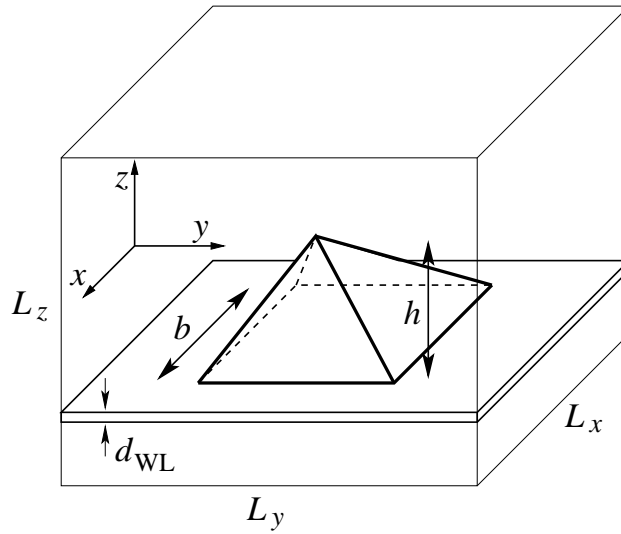


FIG. 1: Quantum dot geometry. The width of the base is b , the height h , the wetting layer width d_{WL} . The embedding box sides are L_x , L_y and L_z . The center of the pyramid base is taken as the origin of the coordinate system.

After multiplying equation (3) from the left by $\frac{1}{(2\pi)^3} \int_V d^3\mathbf{r} \exp(-i\mathbf{q} \cdot \mathbf{r})$, where the integration goes over the volume of the embedding box, using (5) and the identity

$$\int_V d^3\mathbf{r} \exp \left[2i\pi \left(\frac{m_x x}{L_x} + \frac{m_y y}{L_y} + \frac{m_z z}{L_z} \right) \right] = L_x L_y L_z \delta_{m_x,0} \delta_{m_y,0} \delta_{m_z,0}, \quad (6)$$

one arrives at

$$\sum_{j,\mathbf{k}} h_{ij}(\mathbf{q}, \mathbf{k}) A_{j,\mathbf{k}} = E A_{i,\mathbf{q}}, \quad (7)$$

where

$$h_{ij}(\mathbf{q}, \mathbf{k}) = \frac{1}{V} \int_V d^3\mathbf{r} \exp(-i\mathbf{q} \cdot \mathbf{r}) H_{ij} \exp(i\mathbf{k} \cdot \mathbf{r}). \quad (8)$$

The material parameters in \hat{H}_k , \hat{H}_s , \hat{H}_B and \hat{H}_Z are all spatially varying functions since they have different values in the quantum dot and the matrix. Therefore the Hamiltonian matrix h can lose hermiticity unless the proper recipe for the order of differential and

multiplication operators is chosen. This recipe is given by

$$\begin{aligned} f(\mathbf{r})\partial_i\partial_j &\rightarrow \frac{1}{2}(\partial_i f(\mathbf{r})\partial_j + \partial_j f(\mathbf{r})\partial_i), \\ f(\mathbf{r})\partial_i &\rightarrow \frac{1}{2}(\partial_i f(\mathbf{r}) + f(\mathbf{r})\partial_i). \end{aligned} \quad (9)$$

All the elements in the Hamiltonian matrix are a linear combination of the elements of the form $E_1 = f(\mathbf{r})e_{ij}$, $E_2 = f(\mathbf{r})e_{ij}k_l$, $E_3 = f(\mathbf{r})x^\alpha y^\beta$, $E_4 = f(\mathbf{r})x^\alpha y^\beta k_i$ and $E_5 = f(\mathbf{r})x^\alpha y^\beta k_i k_j$, where k_i ($i \in \{1, 2, 3\}$) is the differential operator $k_i = -i\frac{\partial}{\partial x_i}$, e_{ij} are the components of the strain tensor and $f(\mathbf{r})$ is of the form

$$f(\mathbf{r}) = f^{QD}\chi_{QD}(\mathbf{r}) + f^M(1 - \chi_{QD}(\mathbf{r})), \quad (10)$$

where f^{QD} is the value of a material parameter in the quantum dot and f^M its value in the matrix, $\chi_{QD}(\mathbf{r})$ is the quantum dot characteristic function equal to 1 inside the dot and 0 outside the dot. Their Fourier transforms (8) are within the recipe (9) thus given by

$$\tilde{E}_1(\mathbf{q}, \mathbf{k}) = \frac{(2\pi)^3}{V}f^M\tilde{e}_{ij}(\mathbf{q} - \mathbf{k}) - \frac{(2\pi)^6}{V^2}\Delta f \sum_{\mathbf{q}'} \tilde{\chi}_{QD}(\mathbf{q} - \mathbf{k} - \mathbf{q}')\tilde{e}_{ij}(\mathbf{q}'), \quad (11)$$

$$\tilde{E}_2(\mathbf{q}, \mathbf{k}) = \frac{1}{2}(k_l + q_l) \left[\frac{(2\pi)^3}{V}f^M\tilde{e}_{ij}(\mathbf{q} - \mathbf{k}) - \frac{(2\pi)^6}{V^2}\Delta f \sum_{\mathbf{q}'} \tilde{\chi}_{QD}(\mathbf{q} - \mathbf{k} - \mathbf{q}')\tilde{e}_{ij}(\mathbf{q}') \right], \quad (12)$$

$$\tilde{E}_3(\mathbf{q}, \mathbf{k}) = f^M J_{x^\alpha y^\beta}(\mathbf{q} - \mathbf{k}) - \frac{(2\pi)^3}{V}\Delta f \tilde{\chi}_{QD}^{x^\alpha y^\beta}(\mathbf{q} - \mathbf{k}), \quad (13)$$

$$\tilde{E}_4(\mathbf{q}, \mathbf{k}) = \frac{1}{2}(k_i + q_i) \left[f^M J_{x^\alpha y^\beta}(\mathbf{q} - \mathbf{k}) - \frac{(2\pi)^3}{V}\Delta f \tilde{\chi}_{QD}^{x^\alpha y^\beta}(\mathbf{q} - \mathbf{k}) \right], \quad (14)$$

$$\tilde{E}_5(\mathbf{q}, \mathbf{k}) = \frac{1}{2}(k_i q_j + q_i k_j) \left[f^M J_{x^\alpha y^\beta}(\mathbf{q} - \mathbf{k}) - \frac{(2\pi)^3}{V}\Delta f \tilde{\chi}_{QD}^{x^\alpha y^\beta}(\mathbf{q} - \mathbf{k}) \right], \quad (15)$$

where $\Delta f = f^M - f^{QD}$, $\tilde{e}_{ij}(\mathbf{q})$ are Fourier transforms of the strain components given by

$$\tilde{e}_{ij}(\mathbf{q}) = \frac{1}{(2\pi)^3} \int_V d^3\mathbf{r} \exp(-i\mathbf{q} \cdot \mathbf{r}) e_{ij}(\mathbf{r}), \quad (16)$$

$\tilde{\chi}_{QD}^{x^\alpha y^\beta}(\mathbf{q})$ is Fourier transform of the quantum dot characteristic functions

$$\tilde{\chi}_{QD}^{x^\alpha y^\beta}(\mathbf{q}) = \frac{1}{(2\pi)^3} \int_{QD} d^3\mathbf{r} x^\alpha y^\beta \exp(-i\mathbf{q} \cdot \mathbf{r}), \quad (17)$$

where the integration goes only over the volume of the quantum dot and

$$J_{x^\alpha y^\beta}(\mathbf{q} - \mathbf{k}) = \delta_{k_z, q_z} \frac{1}{L_y} \int_{-L_y/2}^{L_y/2} e^{-i(q_y - k_y)y} y^\beta dy \frac{1}{L_x} \int_{-L_x/2}^{L_x/2} e^{-i(q_x - k_x)x} x^\alpha dx, \quad (18)$$

where α and β are non-negative integers from the set

$$(\alpha, \beta) \in \{(0, 0); (1, 0); (2, 0); (0, 1), (1, 1), (0, 2)\}. \quad (19)$$

The center of the pyramid base is taken as the origin of the coordinate system (Fig. 1). The analytical formulae from which $\tilde{e}_{ij}(\mathbf{q})$ can be derived in a crystal with cubic symmetry are given in Ref. 33. After integration, the characteristic functions can all be expressed as a linear combination of integrals of the type

$$I_m(q) = \int_0^{b/2} x^m e^{iqx} dx, \quad (20)$$

where $m \in \{0, 1, 2, 3\}$ and can be therefore evaluated analytically. All the integrals $J_{x^\alpha y^\beta}(\mathbf{q} - \mathbf{k})$ are evaluated analytically, as well.

In order to find the energy levels and the wave functions in the quantum dot, the eigenvalue problem (7) should be solved. The direct application of this approach would lead to an eigenvalue problem of a matrix of size $N \times N$. However, it is possible to exploit the symmetry of the model to block diagonalize the corresponding matrix, as will be done in Sec. II.

II. THE SYMMETRY OF THE MODEL

As already discussed in the introduction, the symmetry group of the model is the double group \overline{C}_4 . The generator of the group is the total angular momentum \hat{F}_z and therefore the representations of the elements of the group are given by the operators $\hat{D}(R(\varphi)) = \exp(-i\varphi\hat{F}_z)$, where $\varphi \in \{k\pi/2\}$ ($k \in \{0, 1, \dots, 7\}$) and $R(\varphi)$ is a rotation by an angle φ . In order to find how operators $\hat{D}(R(\varphi))$ act on the states (Eq. 2), it is enough to find how $\hat{D}(R(\pi/2))$ acts on the states since $\hat{D}(R(k\pi/2)) = \hat{D}(R(\pi/2))^k$. The total angular momentum \hat{F}_z is a sum of the total angular momentum of the Bloch function \hat{J}_z and the orbital angular momentum of the envelope function \hat{L}_z , i.e. $\hat{F}_z = \hat{J}_z + \hat{L}_z$ ²². Therefore action of the operator $\hat{D}(R(\pi/2))$ on state $|\Psi\rangle$ is composed of a rotation of the envelope functions in real space generated by its orbital angular momentum \hat{L}_z and a rotation of the Bloch function generated by its total angular momentum \hat{J}_z

$$\hat{D}(R(\pi/2))|\Psi\rangle = \sum_{i=1}^8 \left[\exp(-i\varphi\hat{L}_z)\psi_i(\mathbf{r}) \right] \left[\exp(-i\varphi\hat{J}_z)|i\rangle \right]. \quad (21)$$

Since the basis of Bloch states $|i\rangle$ is the eigenbasis of \hat{J}_z it follows that

$$\exp(-i\hat{J}_z\pi/2)|i\rangle = \exp(-iJ_z(i)\pi/2)|i\rangle, \quad (22)$$

where $J_z(i)$ is the eigenvalue of the z -component of the total angular momentum of Bloch function $|i\rangle$ ($J_z(1) = -1/2$, $J_z(2) = 1/2$, $J_z(3) = -3/2$, $J_z(4) = -1/2$, $J_z(5) = 1/2$, $J_z(6) = 3/2$, $J_z(7) = -1/2$, $J_z(8) = 1/2$). Thus the operator $\hat{D}(R(\pi/2))$ acts on the state $|\Psi\rangle$ as

$$\hat{D}(R(\pi/2))|\Psi\rangle = \sum_{i=1}^8 \psi_i(y, -x, z) \exp(-iJ_z(i)\pi/2)|i\rangle. \quad (23)$$

By assuming the envelope functions as a linear combination of a finite number of plane waves, we have already reduced the otherwise infinite Hilbert space of the model to the Hilbert space \mathcal{H} of dimension N formed by linear combination of plane waves multiplied by the Bloch functions. The basis of the space \mathcal{H} is given by

$$|\mathbf{k}, i\rangle = \exp(i\mathbf{k} \cdot \mathbf{r})|i\rangle, \quad (24)$$

where $\mathbf{k} = 2\pi \left(\frac{m_x}{L_x}, \frac{m_y}{L_y}, \frac{m_z}{L_z} \right)$, $m_x \in \{-n_x, \dots, n_x\}$, $m_y \in \{-n_y, \dots, n_y\}$, $m_z \in \{-n_z, \dots, n_z\}$ and $i \in \{1, 2, \dots, 8\}$.

We shall first represent the operator $\hat{D}(R(\pi/2))$ in the plane wave basis of the space \mathcal{H} . We thus need to know how $\hat{D}(R(\pi/2))$ acts on the basis vectors. Using (23) and (24) we find that

$$\hat{D}(R(\pi/2))|(k_x, k_y, k_z), i\rangle = \exp(-iJ_z(i)\pi/2)|(-k_y, k_x, k_z), i\rangle. \quad (25)$$

One can note that for $(k_x, k_y) = (0, 0)$ the acting of $\hat{D}(R(\pi/2))$ on the basis vector is just a phase shift and the orbit of acting of the group elements is just an one-dimensional space (we shall denote it as $\mathcal{H}_{(0,0,k_z),i}$), while for $(k_x, k_y) \neq (0, 0)$ the orbit is a four-dimensional space (that we shall denote as $\mathcal{H}_{(k_x,k_y,k_z),i}$, where $k_x > 0$ and $k_y \geq 0$ to avoid multiple counting of the same space) with the basis

$$\begin{aligned} |b1\rangle &= |(k_x, k_y, k_z), i\rangle, \\ |b2\rangle &= |(-k_y, k_x, k_z), i\rangle, \\ |b3\rangle &= |(-k_x, -k_y, k_z), i\rangle, \\ |b4\rangle &= |(k_y, -k_x, k_z), i\rangle. \end{aligned} \quad (26)$$

In the space $\mathcal{H}_{(0,0,k_z),i}$ the representation \hat{D} reduces to an one-dimensional representation defined by

$$\hat{D}_{(0,0,k_z),i}(R(\pi/2)) = \exp(-iJ_z(i)\pi/2), \quad (27)$$

while in the space $\mathcal{H}_{(k_x,k_y,k_z),i}$ it reduces to a four-dimensional representation which is given in the basis from Eq. 26 by

$$\hat{D}_{(k_x,k_y,k_z),i}(R(\pi/2)) = \exp(-iJ_z(i)\pi/2) \begin{bmatrix} 0 & 0 & 0 & 1 \\ 1 & 0 & 0 & 0 \\ 0 & 1 & 0 & 0 \\ 0 & 0 & 1 & 0 \end{bmatrix}. \quad (28)$$

Since the spaces $\mathcal{H}_{(k_x,k_y,k_z),i}$ and $\mathcal{H}_{(0,0,k_z),i}$ are invariant for the representation \hat{D} , it is given by an orthogonal sum

$$\hat{D} = \bigoplus_{k_x, k_y, k_z, i} \hat{D}_{(k_x, k_y, k_z), i} + \bigoplus_{k_z, i} \hat{D}_{(0, 0, k_z), i}. \quad (29)$$

From Eqs. 27 and 28 one finds that the characters of the representation of the group elements are given by

$$\chi \left(\hat{D}_{(k_x, k_y, k_z), i}(R(k\pi/2)) \right) = \begin{cases} 4 & k = 0 \\ -4 & k = 4 \\ 0 & k \in \{1, 2, 3, 5, 6, 7\} \end{cases} \quad (30)$$

and

$$\chi\left(\hat{D}_{(0,0,k_z),i}(R(k\pi/2))\right) = \exp(-iJ_z(i)k\pi/2). \quad (31)$$

The characters of the irreducible representations of the double group \overline{C}_4 are given by $\chi\left(A_{m_f}(R(k\pi/2))\right) = \exp(ikm_f\pi/2)$, where $m_f \in \{-3/2, -1, -1/2, 0, 1/2, 1, 3/2, 2\}$ and $k \in \{0, 1, \dots, 7\}$. One finds from (30) that

$$\hat{D}_{(k_x,k_y,k_z),i} = A_{1/2} + A_{-1/2} + A_{3/2} + A_{-3/2} \quad (32)$$

and from (31) obviously

$$\hat{D}_{(0,0,k_z),i} = A_{-J_z(i)}. \quad (33)$$

Using (32) and (33), it follows from (29) that

$$\hat{D} = N_1 A_{1/2} + N_1 A_{-1/2} + N_2 A_{3/2} + N_2 A_{-3/2}, \quad (34)$$

where

$$N_1 = 8n_x(n_y + 1)(2n_z + 1) + 3(2n_z + 1) \quad (35)$$

and

$$N_2 = 8n_x(n_y + 1)(2n_z + 1) + 2n_z + 1. \quad (36)$$

Projection operators¹⁷ were then used to find the symmetry adapted basis. The projection operators are given by

$$\hat{P}_{A_{m_f}}((k_x, k_y, k_z), i) = \frac{1}{8} \sum_{k=0}^7 \chi\left(A_{m_f}(R(k\pi/2))\right)^* \hat{D}_{(k_x,k_y,k_z),i}(R(k\pi/2)), \quad (37)$$

while

$$\hat{P}_{A_{m_f}}((0, 0, k_z), i) = 1 \quad (38)$$

and they project arbitrary states in space \mathcal{H} to the elements of the symmetry adapted basis. The explicit forms of the projection operators are derived from (37) and (28) and in the basis (26) are equal to

$$\begin{aligned} \hat{P}_{A_{-3/2}}(1) &= \hat{P}_{A_{-3/2}}(4) = \hat{P}_{A_{-3/2}}(7) = \hat{P}_{A_{-1/2}}(3) = \\ &= \hat{P}_{A_{1/2}}(6) = \hat{P}_{A_{3/2}}(2) = \hat{P}_{A_{3/2}}(5) = \hat{P}_{A_{3/2}}(8) = M_1, \\ \hat{P}_{A_{-3/2}}(2) &= \hat{P}_{A_{-3/2}}(5) = \hat{P}_{A_{-3/2}}(8) = \hat{P}_{A_{-1/2}}(1) = \\ &= \hat{P}_{A_{-1/2}}(4) = \hat{P}_{A_{-1/2}}(7) = \hat{P}_{A_{1/2}}(3) = \hat{P}_{A_{3/2}}(6) = M_2, \\ \hat{P}_{A_{-3/2}}(6) &= \hat{P}_{A_{-1/2}}(2) = \hat{P}_{A_{-1/2}}(5) = \hat{P}_{A_{-1/2}}(8) = \\ &= \hat{P}_{A_{1/2}}(1) = \hat{P}_{A_{1/2}}(4) = \hat{P}_{A_{1/2}}(7) = \hat{P}_{A_{3/2}}(3) = M_3, \\ \hat{P}_{A_{-3/2}}(3) &= \hat{P}_{A_{-1/2}}(6) = \hat{P}_{A_{1/2}}(2) = \hat{P}_{A_{1/2}}(5) = \\ &= \hat{P}_{A_{1/2}}(8) = \hat{P}_{A_{3/2}}(1) = \hat{P}_{A_{3/2}}(4) = \hat{P}_{A_{3/2}}(7) = M_4, \end{aligned} \quad (39)$$

where (k_x, k_y, k_z) was omitted in all brackets for brevity and where the matrices $M_1, M_2,$

M_3 and M_4 are given by

$$M_1 = \frac{1}{4} \begin{bmatrix} 1 & -1 & 1 & -1 \\ -1 & 1 & -1 & 1 \\ 1 & -1 & 1 & -1 \\ -1 & 1 & -1 & 1 \end{bmatrix}, \quad M_2 = \frac{1}{4} \begin{bmatrix} 1 & -i & -1 & i \\ i & 1 & -i & -1 \\ -1 & i & 1 & -i \\ -i & -1 & i & 1 \end{bmatrix},$$

$$M_3 = \frac{1}{4} \begin{bmatrix} 1 & 1 & 1 & 1 \\ 1 & 1 & 1 & 1 \\ 1 & 1 & 1 & 1 \\ 1 & 1 & 1 & 1 \end{bmatrix}, \quad M_4 = \frac{1}{4} \begin{bmatrix} 1 & i & -1 & -i \\ -i & 1 & i & -1 \\ -1 & -i & 1 & i \\ i & -1 & -i & 1 \end{bmatrix}. \quad (40)$$

The elements of the symmetry adapted basis are finally given as:

$$\begin{aligned} |A_{1/2}, (0, 0, k_z), i\rangle &= |(0, 0, k_z), i\rangle & i \in \{1, 4, 7\} \\ |A_{1/2}, (k_x, k_y, k_z), i\rangle &= \frac{1}{2} (|b1\rangle + |b2\rangle + |b3\rangle + |b4\rangle) & i \in \{1, 4, 7\} \\ |A_{1/2}, (k_x, k_y, k_z), i\rangle &= \frac{1}{2} (|b1\rangle - i|b2\rangle - |b3\rangle + i|b4\rangle) & i \in \{2, 5, 8\} \\ |A_{1/2}, (k_x, k_y, k_z), i\rangle &= \frac{1}{2} (|b1\rangle - |b2\rangle + |b3\rangle - |b4\rangle) & i = 6 \\ |A_{1/2}, (k_x, k_y, k_z), i\rangle &= \frac{1}{2} (|b1\rangle + i|b2\rangle - |b3\rangle - i|b4\rangle) & i = 3, \end{aligned} \quad (41)$$

$$\begin{aligned} |A_{-1/2}, (0, 0, k_z), i\rangle &= |(0, 0, k_z), i\rangle & i \in \{2, 5, 8\} \\ |A_{-1/2}, (k_x, k_y, k_z), i\rangle &= \frac{1}{2} (|b1\rangle + |b2\rangle + |b3\rangle + |b4\rangle) & i \in \{2, 5, 8\} \\ |A_{-1/2}, (k_x, k_y, k_z), i\rangle &= \frac{1}{2} (|b1\rangle - i|b2\rangle - |b3\rangle + i|b4\rangle) & i = 6 \\ |A_{-1/2}, (k_x, k_y, k_z), i\rangle &= \frac{1}{2} (|b1\rangle - |b2\rangle + |b3\rangle - |b4\rangle) & i = 3 \\ |A_{-1/2}, (k_x, k_y, k_z), i\rangle &= \frac{1}{2} (|b1\rangle + i|b2\rangle - |b3\rangle - i|b4\rangle) & i \in \{1, 4, 7\}, \end{aligned} \quad (42)$$

$$\begin{aligned} |A_{-3/2}, (0, 0, k_z), i\rangle &= |(0, 0, k_z), i\rangle & i = 6 \\ |A_{-3/2}, (k_x, k_y, k_z), i\rangle &= \frac{1}{2} (|b1\rangle + |b2\rangle + |b3\rangle + |b4\rangle) & i = 6 \\ |A_{-3/2}, (k_x, k_y, k_z), i\rangle &= \frac{1}{2} (|b1\rangle - i|b2\rangle - |b3\rangle + i|b4\rangle) & i = 3 \\ |A_{-3/2}, (k_x, k_y, k_z), i\rangle &= \frac{1}{2} (|b1\rangle - |b2\rangle + |b3\rangle - |b4\rangle) & i \in \{1, 4, 7\} \\ |A_{-3/2}, (k_x, k_y, k_z), i\rangle &= \frac{1}{2} (|b1\rangle + i|b2\rangle - |b3\rangle - i|b4\rangle) & i \in \{2, 5, 8\}, \end{aligned} \quad (43)$$

$$\begin{aligned} |A_{3/2}, (0, 0, k_z), i\rangle &= |(0, 0, k_z), i\rangle & i = 3 \\ |A_{3/2}, (k_x, k_y, k_z), i\rangle &= \frac{1}{2} (|b1\rangle + |b2\rangle + |b3\rangle + |b4\rangle) & i = 3 \\ |A_{3/2}, (k_x, k_y, k_z), i\rangle &= \frac{1}{2} (|b1\rangle - i|b2\rangle - |b3\rangle + i|b4\rangle) & i \in \{1, 4, 7\} \\ |A_{3/2}, (k_x, k_y, k_z), i\rangle &= \frac{1}{2} (|b1\rangle - |b2\rangle + |b3\rangle - |b4\rangle) & i \in \{2, 5, 8\} \\ |A_{3/2}, (k_x, k_y, k_z), i\rangle &= \frac{1}{2} (|b1\rangle + i|b2\rangle - |b3\rangle - i|b4\rangle) & i = 6. \end{aligned} \quad (44)$$

The Hamiltonian matrix elements between basis elements having different symmetry are equal to zero implying that in this basis the Hamiltonian matrix is block diagonal with four blocks of sizes $N_1 \times N_1$, $N_1 \times N_1$, $N_2 \times N_2$ and $N_2 \times N_2$, respectively. The time necessary

to diagonalize the matrix of size $N \times N$ scales approximately as N^3 . Therefore the block diagonalization obtained reduces the computational time approximately by a factor of 16. Since all the basis vectors of the symmetry adapted basis are linear combinations of one or four vectors of the plane wave basis, it follows that Hamiltonian matrix elements in the symmetry adapted basis can be expressed as linear combinations of one, four or sixteen Hamiltonian matrix elements in the plane wave basis. Therefore all the elements of the four blocks are given by analytical formulae that can be easily derived from the analytical formulae for the matrix elements in the plane wave basis given in Sec. I.

It can be proved by considering the two dimensional irreducible representations of the more general double group \overline{C}_{4v} ¹⁷ that states with the same absolute value of m_f are degenerate in pairs (the Kramer's degeneracy). This degeneracy is lifted in the presence of external axial magnetic field B when the symmetry reduces from \overline{C}_{4v} to \overline{C}_4 and the time reversal symmetry relation $E_{m_f}(B) = E_{-m_f}(-B)$ holds then.

It has been pointed out^{34,35} that piezoelectric effects in single dots of realistic sizes are small, changing the eigen-energies of the system by less than 1 meV, and can be neglected. It has also been shown that in a vertically stacked double quantum dot the influence of a piezoelectric field is more important since the piezoelectric potential generated by the two dots adds up in the regions above and below the dots, while it is almost cancelled out in the region between the dots. Consequently, it is expected that in a periodic array of vertically stacked quantum dots considered in Sec. III the piezoelectric potential in the region between the dots would be almost cancelled out and that the influence of piezoelectric effect on eigen-energies would be small. Therefore the small piezoelectric potential that breaks the symmetry of the system from \overline{C}_4 to \overline{C}_2 can be treated as a perturbation. It belongs to the A_2 representation of \overline{C}_4 group and therefore only the matrix elements between the states with $\Delta m_f = 2$ are non zero. Consequently, the piezoelectric potential doesn't change the energies in the first order of the perturbation theory and second order perturbation theory is needed to take the piezoelectric effect into account.

We introduce the following notation for the electron states ne_{m_f} , where n is a positive integer labeling the states with given m_f in increasing order of their energy. Since the quantum number m_f originates from the irreducible representations of the double group \overline{C}_4 whose elements are generated by the total angular momentum, its physical interpretation is that it represents the total quasi-angular momentum. The hole states will be labeled by nh_{m_f} , with the same meaning of the symbol as for the electron case, except that n labels the states in decreasing order of their energy, as is natural for holes.

The Hamiltonian of the interaction with the electromagnetic field is obtained by replacing \mathbf{k} with $\mathbf{k} + \frac{e}{\hbar}\mathbf{A}$ in the kinetic part of the Hamiltonian. In the dipole approximation \mathbf{A} can be considered constant in space and furthermore all the terms quadratic in \mathbf{A} are neglected. After calculating the matrix elements between states with a well defined symmetry, we obtain the following selection rules. If the light is z -polarized then $\Delta m_f = 0$, while if the light is σ^\pm circularly polarized then $\Delta m_f = \pm 1$ (where by definition $3/2 + 1 = -3/2$ and $-3/2 - 1 = 3/2$).

III. RESULTS

The method presented was applied to the calculation of the electronic structure of periodic array of vertically stacked pyramidal self-assembled quantum dots (Fig. 2). The dimensions of the dots in an array were taken to be equal to those estimated for the structure reported

in Ref. 19 - the base width $b = 18$ nm, the height $h = 4$ nm, the wetting layer width $d_{WL} = 1.7ML$, while the period of the structure in z -direction L_z was varied in the interval from $L_z = h + d_{WL}$ where the dots lie on top of one another to $L_z = 16$ nm. The dimensions of the embedding box $L_x = L_y = 2b$ were taken. The material parameters were taken from Ref. 36. According to Bloch's theorem, the k -th component of the state spinor is given by

$$\Psi_k(\mathbf{r}) = \exp(iK_z z)\psi_k(\mathbf{r}), \quad (45)$$

where $k \in \{1, 2, \dots, 8\}$ and $\psi_k(\mathbf{r})$ is periodic in the z -direction with the period L_z . Therefore, the matrix elements in the four blocks of the Hamiltonian matrix for calculating $E(K_z)$ are given by linear combinations of the elements obtained by the same formulae from Sec. I except that k_z and q_z should be replaced by $k_z + K_z$ and $q_z + K_z$, respectively. Since the relation $E(K_z) = E(-K_z)$ holds, only the states with $K_z \geq 0$ will be considered. The InAs unstrained conduction band edge is taken as the energy reference level.

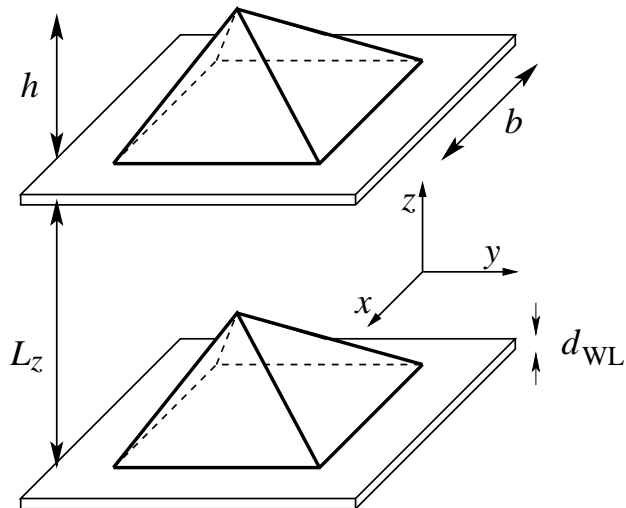


FIG. 2: Geometry of a periodic array of pyramidal quantum dots. The width of the pyramid base is b , the height h , the wetting layer width d_{WL} , the period of the structure is L_z .

The small piezoelectric effect was assumed to be negligible in the calculation. In order to check this assumption it was included in the framework of second order perturbation theory (Sec. II). Its influence on the state energies was of the order of 1 meV and less, confirming our assumption.

Two main factors influence the electronic structure of the periodic array of quantum dots - strain distribution and quantum mechanical coupling.

The influence of quantum mechanical coupling is intuitively clear - as the distance between the dots increases the coupling is weaker implying smaller miniband widths. Due to their large effective mass, heavy-holes are the least influenced by coupling and the minibands of dominantly heavy-hole like states are narrow, while the minibands of electron and light-hole states are much wider.

On the other hand, the strain distribution is complex and in principle all six components of the strain tensor influence the electronic structure. Still, the most important are hydrostatic

strain $e_h = e_{11} + e_{22} + e_{33}$ that determines the position of the electron and hole levels and biaxial strain $e_b = e_{33} - \frac{1}{2}(e_{11} + e_{22})$ whose main influence is on splitting of the light and heavy-hole states. The bigger the value of hydrostatic strain, the lower the conduction band states are in energy and the higher the valence band states are in energy. When the biaxial strain is negative, the light-holes tend to have higher energy than heavy-holes, while when it is positive the situation is opposite. Having the importance of those two components of strain in mind, we have investigated first how they change when the distance between the dots in an array is varied. We have found that as the distance between the dots increases, the hydrostatic strain in the dots decreases. On the other hand, for small values of the period, the biaxial strain is negative, while for larger values it changes sign and increases further.

A. Energy levels in the conduction band

The dependence of the miniband minima and maxima on the period of the structure is given in Fig. 3. This behavior is expected. When the dots are close, they are strongly coupled and the minibands are wide, while as L_z increases the coupling is weaker and the energy spectrum becomes discrete. For large values of the period when the miniband width practically vanishes, we still see a rising trend in energy. This rise is caused by a still decreasing value of hydrostatic strain. This leads us to the conclusion that the range of strain effects is larger than the range of quantum mechanical coupling.

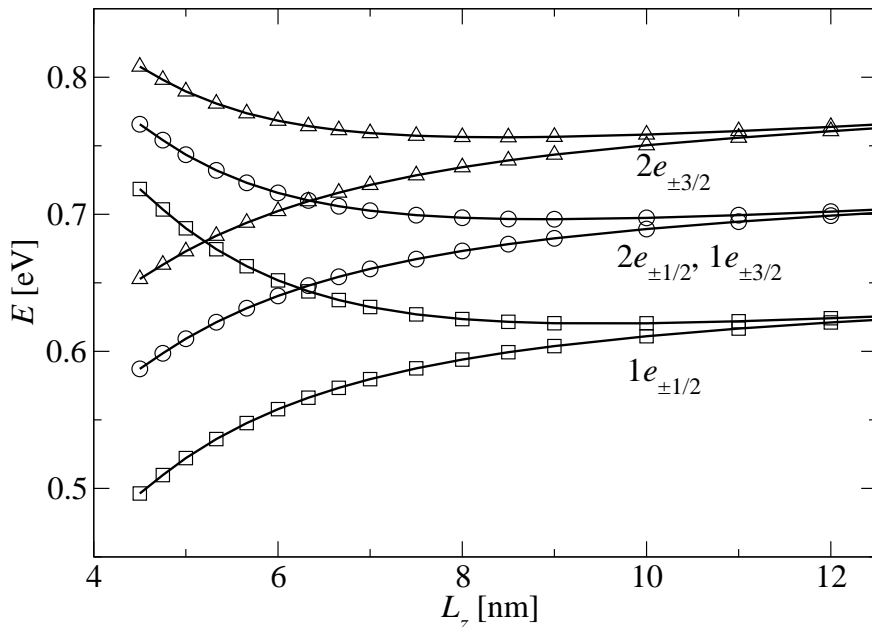


FIG. 3: The conduction miniband minima and maxima dependence on the period of the structure L_z . The $1e_{\pm 1/2}$ miniband is represented by squares, the $1e_{\pm 3/2}$ and $2e_{\pm 1/2}$ miniband by circles, the $2e_{\pm 3/2}$ miniband by triangles.

The ground miniband has $|m_f| = 1/2$ symmetry, while the first and second excited

miniband having different symmetries $|m_f| = 1/2$ and $|m_f| = 3/2$ are nearly degenerate. Their difference in energy is less than 1 meV, too small to be seen on the graph. A comment should be given about the near degeneracy of those two states. It has been practice in the literature to say that these two states are exactly degenerate in the absence of a piezoelectric effect and that the piezoelectric effect breaks the degeneracy of these states. This is indeed true if the carrier energy spectrum in the quantum dot is modeled by simple one band Schrödinger equation. The symmetry group is then C_{4v} , consisting of transformations in real space generated by the orbital angular momentum \hat{L}_z and the first and second excited state transform according to the same two dimensional irreducible representation of C_{4v} implying their degeneracy. However, when the 8-band $k \cdot p$ model, which is inherently spin-dependent, is used, the Hamiltonian no longer commutes with the rotations generated by orbital angular momentum, but the total angular momentum. The symmetry group is the double \overline{C}_4 group that has only the one dimensional irreducible representations and there is no a priori reason for the states with different absolute values of m_f to be degenerate.

In order to explain the near degeneracy of the states with different symmetry, we have further investigated the 8-band $k \cdot p$ Hamiltonian and checked that it would still commute with the transformations in real space generated by orbital angular momentum if the valence band spin-orbit splitting would be set to zero. Since the influence of valence band spin-orbit splitting on the levels in the conduction band is not substantial, the degeneracy of the two states is small. We thus conclude that the origin of splitting of the first and the second excited state is not just the piezoelectric effect but also the valence band spin-orbit splitting.

All the minibands shown in Fig. 3 exhibit minima at $K_z = 0$ and maxima at $K_z = \pi/L_z$ for all values of the period L_z . For small values of the period L_z there is an energy overlap between different minibands, while the minibands are completely separated for larger values of L_z . There is no crossing between states of different symmetry.

B. Energy levels in the valence band

The miniband minima and maxima dependence on the period of the structure are given in Fig. 4 for the three highest minibands in the valence band. Due to the combined effects of strain, mixing of light and heavy-holes and quantum mechanical coupling between the dots, the hole minibands exhibit a more complex structure than the electron minibands.

In order to explain such behavior we note first that the effective potential felt by carriers depends on K_z . We define the effective potential as the value obtained by diagonalizing the Hamiltonian with $k_x = k_y = 0$ and $k_z = K_z$. The z -dependence of electron, light, heavy and spin-orbit split hole $K_z = 0$ and $K_z = \pi/L_z$ effective potentials at the pyramid axis for a few different values of L_z is shown in Fig. 5.

Since the effective mass of the light-holes is small, the light-hole effective potential is substantially different for $K_z = 0$ and $K_z = \pi/L_z$, while in the case of heavy-holes that difference is much smaller. As seen from Fig. 5, as the period of the structure increases, the effective potential felt by $K_z = 0$ light-holes decreases, while quite oppositely the effective potential felt by heavy-holes increases. Both of these trends are an expected consequence of the increase in the value of the biaxial strain. Consequently, in the range of low values of L_z the hole states with $K_z = 0$ are dominantly of the light-hole type, while the states with $K_z = \pi/L_z$ are dominantly heavy-hole like. The states with $K_z = \pi/L_z$ remain of heavy-hole type across the whole investigated interval of L_z and their energy therefore increases with increasing L_z . The energy of the light-hole $K_z = 0$ states decreases with increasing L_z

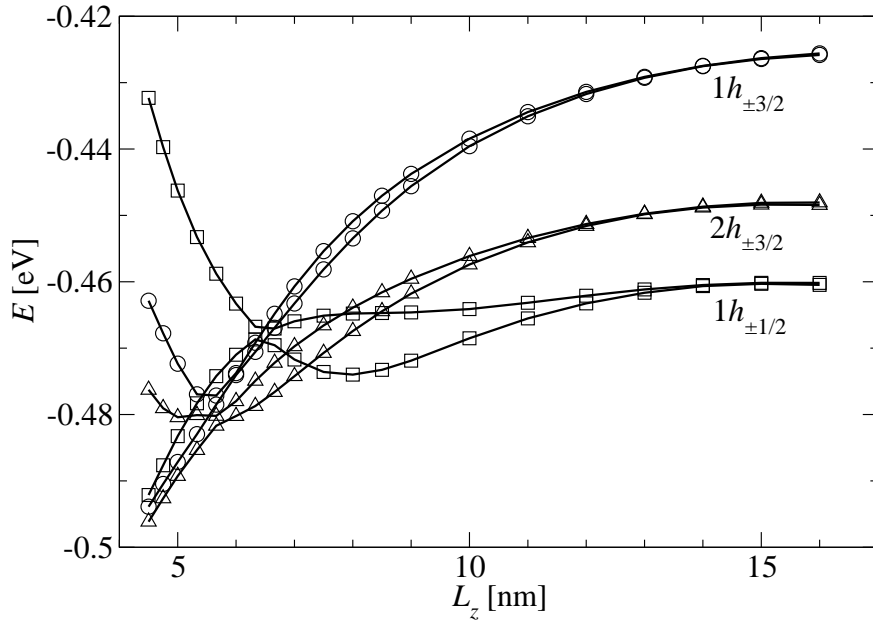


FIG. 4: The miniband minima and maxima dependence on the period of the structure L_z . The $1h_{\pm 1/2}$ miniband is represented by squares, the $1h_{\pm 3/2}$ miniband by circles and the $2h_{\pm 3/2}$ miniband by triangles.

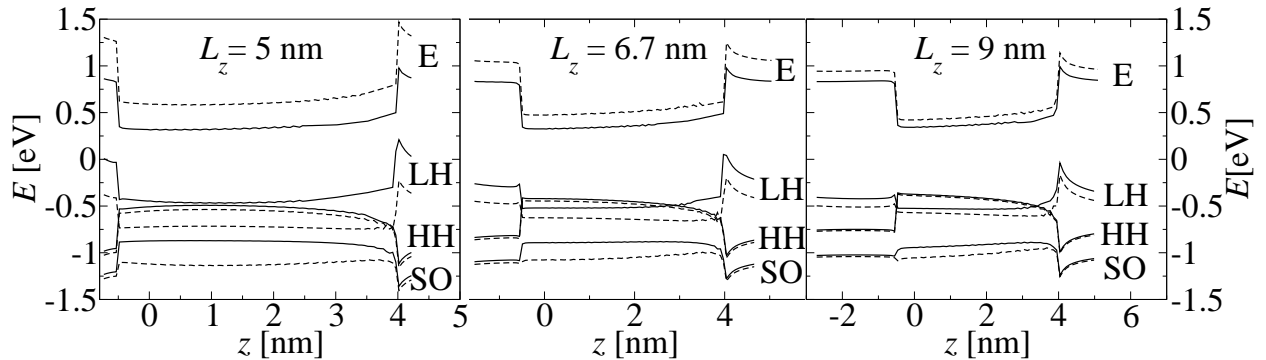


FIG. 5: Effective potentials at three different values of the period L_z at $K_z = 0$ (full lines) and $K_z = \pi/L_z$ (dashed lines) for electrons (E), light-holes (LH), heavy-holes (HH) and spin orbit split holes (SO).

and at the same time their heavy-hole content increases. As a consequence of two different energy trends for $K_z = 0$ and $K_z = \pi/L_z$ the miniband width decreases for all the states until a certain point where the energy of the $K_z = 0$ state becomes less than the energy of the $K_z = \pi/L_z$ state. This point, where the inversion of the sign of the miniband effective mass occurs is different for different states, for the $1h_{\pm 1/2}$ state it occurs around $L_z = 6.5$ nm, while for the $1h_{\pm 3/2}$ and $2h_{\pm 3/2}$ states it occurs around $L_z = 5.8$ nm. The light-hole content

of the $K_z = 0$ states decreases with increasing L_z and eventually they become dominantly heavy-hole like. This light to heavy-hole transition occurs at $L_z = 7.5$ nm for the $1h_{\pm 1/2}$ state, at $L_z = 5.5$ nm for the $1h_{\pm 3/2}$ state and $L_z = 5.0$ nm for the $2h_{\pm 3/2}$ state. Since the energy of the light-hole states decreases with increasing L_z and the energy of the heavy-hole states increases, the position of the light to heavy-hole transition corresponds approximately to the position of the energy minima of $K_z = 0$ states, as can be verified from Fig. 4. We further observe that the ground hole state for $L_z \leq 6.5$ nm is $1h_{\pm 1/2}$ having $|m_f| = 1/2$ symmetry, while for $L_z > 6.5$ nm it is $1h_{\pm 3/2}$ having $|m_f| = 3/2$ symmetry. Therefore at the critical point $L_z = 6.5$ nm, we observe an interesting effect of a simultaneous change of ground hole state symmetry, a change of the sign of the effective mass and a change of the ground state type from light to heavy-hole like.

The spin orbit split band certainly influences the exact positions of the energy levels, however, being far in energy from the light and heavy-hole bands it doesn't influence the overall behavior described in the previous paragraph. This is verified by the fact that the spin orbit band content of the hole states is typically of the order of 5%.

As far as the spatial localization of the wave functions is concerned, one would expect from the effective potential profiles given in Fig. 5 that dominantly light-hole states would be confined outside the dots and dominantly heavy-hole states inside the dots. However, the states are of light-hole type only when the dots are very close to each other and the effective potential well is then too narrow to confine the hole. Therefore, the light-hole like states are spread both inside and outside the dots. When the distance between the dots increases and light to heavy-hole transitions take place, the hole state becomes localized inside the dots.

C. Influence of external axial magnetic field

The magnetic field dependences of the miniband minima and maxima of the conduction and valence band states for the structure with the period $L_z = 6$ nm are shown in Figs. 6 and 7, respectively. As already mentioned, Kramer's degeneracy is broken in magnetic field. The relation $E_{m_f}(B) = E_{-m_f}(-B)$ holds, thus only the $B \geq 0$ part of the dependence is shown on the graphs.

The magnetic field splitting between $1e_{+3/2}$ and $1e_{-3/2}$ states, as well as between $2e_{-1/2}$ and $2e_{+1/2}$ states is significant because the mesoscopic angular momentum²³ of those states is different from zero. However, the splitting between $1e_{-1/2}$ and $1e_{+1/2}$ states and between $2e_{+3/2}$ and $2e_{-3/2}$ is much smaller, too small to be seen on the graph (of the order of few meV). There is no crossing between the states of different symmetry. We also note that the $1e_{+1/2}$ and $1e_{-1/2}$ minibands overlap with $2e_{-1/2}$ and $1e_{-3/2}$ minibands for $B = 0$ but as the magnetic field is increased this overlap vanishes (for $B \gtrsim 12$ T). The energy separation of the minibands has an important affect on the dynamical characteristics of the structure since it suppresses all the one particle energy conserving scattering mechanisms between those minibands (like ionized impurity scattering) and with further separation even suppresses the mechanisms with energy exchange (like acoustic phonon and longitudinal optical phonon scattering).

The splitting between the hole states is also of the order of a few meV, however since the energy difference between different states is also small, this splitting is enough to cause crossings between states of different symmetry. We further find from Fig. 7 that the minibands $1h_{-3/2}$ and $1h_{+3/2}$ that are degenerate at $B = 0$ become completely separated already at $B \gtrsim 3$ T and the same effect for $2h_{-3/2}$ and $2h_{+3/2}$ occurs at $B \gtrsim 23$ T. Although the

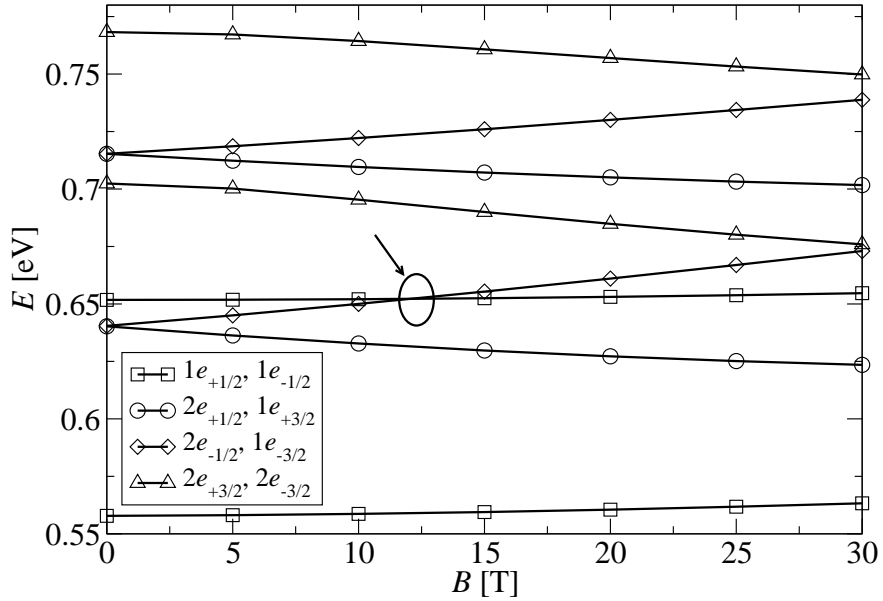


FIG. 6: Magnetic field dependence of miniband minima and maxima for $1e_{-3/2}$, $1e_{-1/2}$, $1e_{+1/2}$, $1e_{+3/2}$, $2e_{-3/2}$, $2e_{-1/2}$, $2e_{+1/2}$ and $2e_{+3/2}$ states. The position where different minibands separate is marked.

magnetic field splitting is the most pronounced for $1h_{-1/2}$ and $1h_{+1/2}$ states, the effect of the separation of those minibands occurs at magnetic fields larger than 30 T, which is a consequence of larger miniband width than in the previous cases. Apart from separation of the minibands, the magnetic field can also concatenate otherwise nonoverlapping minibands. It is seen in Fig. 7 that $1h_{+1/2}$ and $1h_{-3/2}$ start to overlap at $B \sim 11$ T and that for $B \gtrsim 22$ T the range of energies of $1h_{-3/2}$ becomes a subset of the range of energies of $1h_{+1/2}$ miniband.

IV. CONCLUSION

In conclusion, we have developed a symmetry-based method for calculation of electronic states in pyramidal InAs/GaAs quantum dots. The corresponding Hamiltonian matrix obtained by the plane wave method was block diagonalized into four matrices of approximately equal size, which enabled significantly faster calculation of energy levels within the plane wave method. The symmetry considerations not only enabled more efficient calculation of the electronic structure but also give more insight about the physics of the model by introducing the quantum number of total quasi-angular momentum and giving the selection rules for interaction with electromagnetic field. The method developed was applied to calculate the electronic structure of a periodic array of vertically stacked pyramidal self-assembled quantum dots. It was found that as the distance between the dots is increased, at a certain critical point the ground hole state simultaneously changes symmetry from $|m_f| = 1/2$ to $|m_f| = 3/2$ and type from light to heavy-hole. The influence of magnetic field on the energy levels is in general less pronounced than the influence of quantum mechanical coupling and strain but nevertheless it can be used for fine tuning of the properties of the structure since

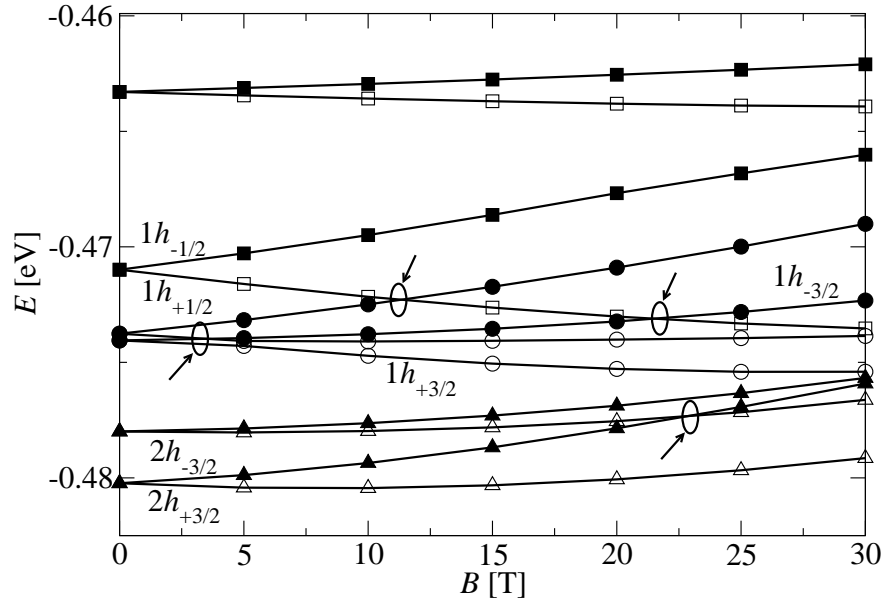


FIG. 7: Magnetic field dependence of miniband minima and maxima for $1h_{-3/2}$ (full circles), $1h_{+3/2}$ (empty circles), $1h_{-1/2}$ (full squares), $1h_{+1/2}$ (empty squares), $2h_{-3/2}$ (full triangles) and $2e_{+3/2}$ (empty triangles) states. The positions where different minibands separate or concatenate are marked.

its increase or decrease is able to separate energy overlapping minibands.

* Electronic address: eennv@leeds.ac.uk

- ¹ J. Oshinowo, M. Nishioka, S. Ishida, and Y. Arakawa, Appl. Phys. Lett. **65**, 1421 (1994).
- ² D. Leonard, M. Krishnamurthy, C. M. Reaves, S. P. Denbaars, and P. M. Petroff, Appl. Phys. Lett. **63**, 3203 (1993).
- ³ M. Bayer, P. Hawrylak, K. Hinzer, S. Fafard, M. Korkusinski, Z. R. Wasilewski, O. Stern, and A. Forchel, Science **291**, 451 (2001).
- ⁴ J. Y. Marzin and G. Bastard, Solid State Commun. **92**, 437 (1994).
- ⁵ M. Califano and P. Harrison, Phys. Rev. B **61**, 10959 (2000).
- ⁶ J. A. Barker and E. P. O'Reilly, Phys. Rev. B **61**, 13840 (2000).
- ⁷ M. A. Cusack, P. R. Briddon, and M. Jaros, Phys. Rev. B **54**, R2300 (1996).
- ⁸ O. Stier, M. Grundmann, and D. Bimberg, Phys. Rev. B **59**, 5688 (1999).
- ⁹ C. Pryor, Phys. Rev. Lett. **80**, 3579 (1998).
- ¹⁰ H. Jiang and J. Singh, Phys. Rev. B **56**, 4696 (1997).
- ¹¹ C. Pryor, Phys. Rev. B **57**, 7190 (1998).
- ¹² L. W. Wang, J. Kim, and A. Zunger, Phys. Rev. B **59**, 5678 (1999).
- ¹³ G. Bester and A. Zunger, Phys. Rev. B **71**, 045318 (2005).
- ¹⁴ M. Tadić, F. M. Peeters, and K. L. Janssens, Phys. Rev. B **65**, 165333 (2002).
- ¹⁵ P. Tronc, V. P. Smirnov, and K. S. Zhuravlev, Phys. Status Solidi B **241**, 2938 (2004).

- ¹⁶ M. Roy and P. A. Maksym, Phys. Rev. B **68**, 235308 (2003).
- ¹⁷ J. P. Elliott and P. G. Dawber, *Symmetry in Physics* (Macmillan, London, 1979).
- ¹⁸ M. Tadić, F. M. Peeters, K. L. Janssens, M. Korkusiński, and P. Hawrylak, J. Appl. Phys. **92**, 5819 (2002).
- ¹⁹ G. S. Solomon, J. A. Trezza, A. F. Marshall, and J. S. Harris, Jr., Phys. Rev. Lett. **76**, 952 (1996).
- ²⁰ P. Yu, W. Langbein, K. Leosson, J. M. Hvam, N. N. Ledentsov, D. Bimberg, V. M. Ustinov, A. Y. Egorov, A. E. Zhukov, A. F. Tsatsul'nikov, et al., Phys. Rev. B **60**, 16680 (1999).
- ²¹ S.-S. Li and J.-B. Xia, Phys. Rev. B **58**, 3561 (1998).
- ²² F. B. Pedersen and Y.-C. Chang, Phys. Rev. B **55**, 4580 (1997).
- ²³ M. Brasken, M. Lindberg, and J. Tulkki, Phys. Rev. B **55**, 9275 (1997).
- ²⁴ D. Bellucci, M. Rontani, F. Troiani, G. Goldoni, and E. Molinari, Phys. Rev. B **69**, 201308(R) (2004).
- ²⁵ E. Anisimovas and F. M. Peeters, Phys. Rev. B **68**, 115310 (2003).
- ²⁶ Y. B. Lyanda-Geller, T. L. Reinecke, and M. Bayer, Phys. Rev. B **69**, 161308(R) (2004).
- ²⁷ D. Jacob, B. Wunsch, and D. Pfannkuche, Phys. Rev. B **70**, 081314(R) (2004).
- ²⁸ M. Korkusiński and P. Hawrylak, Phys. Rev. B **63**, 195311 (2001).
- ²⁹ T. Nakaoka, T. Saito, J. Tatebayashi, and Y. Arakawa, Phys. Rev. B **70**, 235337 (2004).
- ³⁰ A. D. Andreev and E. P. O'Reilly, Phys. Rev. B **62**, 15851 (2000).
- ³¹ T. B. Bahder, Phys. Rev. B **41**, 11992 (1990).
- ³² L. R. Ram-Mohan, K. H. Yoo, and R. L. Aggarwal, Phys. Rev. B **38**, 6151 (1988).
- ³³ A. D. Andreev, J. R. Downes, D. A. Faux, and E. P. O'Reilly, J. Appl. Phys. **86**, 297 (1999).
- ³⁴ L. R. C. Fonseca, J. L. Jimenez, and J. P. Leburton, Phys. Rev. B **58**, 9955 (1998).
- ³⁵ M. Grundmann, O. Stier, and D. Bimberg, Phys. Rev. B **52**, 11969 (1995).
- ³⁶ I. Vurgaftman, J. R. Meyer, and L. R. Ram-Mohan, J. Appl. Phys. **89**, 5815 (2001).